Hindawi
Modelling and Simulation in Engineering
Volume 2018, Article ID 2687561, 20 pages
https://doi.org/10.1155/2018/2687561

Research Article

Collapse Analysis of Transmission Tower Subjected to Earthquake Ground Motion

Xiaohong Long,[1,2] **Wei Wang**,[1,2] **and Jian Fan**[1,2]

[1] *School of Civil Engineering and Mechanics, Huazhong University of Science and Technology, Wuhan 430074, China*
[2] *Hubei Key Laboratory of Control Structure, Huazhong University of Science and Technology, Wuhan 430074, China*

Correspondence should be addressed to Xiaohong Long; xhlong@hust.edu.cn

Received 24 August 2017; Revised 3 November 2017; Accepted 5 December 2017; Published 20 February 2018

Academic Editor: Zhiping Qiu

The collapse of transmission towers involves a series of complex problems, including geometric nonlinearity, material nonlinearity, dynamic nonlinearity, and the failure of members. Simulation of the process of collapse is difficult using traditional finite element method (FEM), which is generated from continuum and variation principle, whereas the finite particle method (FPM) enforces equilibrium on each point. Particles are free to separate from one another, which is advantageous in the simulation of the structural collapse. This paper employs the finite particle method (FPM) to simulate the collapse of a transmission steel tower under earthquake ground motions; the three-dimensional (3D) finite particle model using MATLAB and the 3D finite element model using ANSYS of the transmission steel tower are established, respectively. And the static and elastic seismic response analyses indicate that the results of the FPM agree well with those of the FEM. To simulate the collapse of the transmission steel tower, a failure criterion based on the ideal elastic-plastic model and a failure mode are proposed. Finally, the collapse simulation of the transmission steel towers subjected to unidirectional earthquake ground motion and the collapse seismic fragility analysis can be successfully carried out using the finite particle method. The result indicates that the transmission steel tower has better seismic safety performance and anticollapse ability.

1. Introduction

The breakdown or collapse of transmission towers is common during an earthquake. In the United States, the Landers earthquake in 1992 and the Northridge earthquake in 1994 severely damaged the transmission system, respectively [1]. The Kobe earthquake in Japan in 1955 resulted in the destruction of a large number of transmission towers whose main failure modes were the subsidence of foundation, the tilt of tower, and compressive yield of structural member [2]. The Kocaeli earthquake in Turkey in 1999 also caused landslides, faulting, and ruptures of earth's surface, thereby damaging a considerable number of transmission towers [3]. Moreover, transmission lines also broke down in the Wenchuan earthquake in China in 2008 [4–6]. Figure 1 depicts the collapse of transmission towers during the earthquake.

The seismic dynamic responses of transmission towers involve initially solving a mechanical model, and its analysis involves many nonlinear problems, such as dynamic nonlinearity, geometric nonlinearity, and material nonlinearity. Kempner et al. [7] analyzed the structure of transmission towers by using the space frame model or the space truss model and discovered that the damping ratio of a 45 m high transmission tower varied between 0.015 and 0.04. Meanwhile, Kitipornchai et al. [8, 9] and Meek et al. [10, 11] established a space rigid frame model to analyze the correlations of transmission towers. They deduced the element stiffness matrix by considering initial stress, initial deformation, and geometry. The results of numerical simulation were highly consistent with those of structural tests, and they significantly improved the computational efficiency. Yasui et al. [12] established a finite element model by using the beam element and the truss element and conducted a dynamic response analysis of self-supporting and guyed transmission towers induced by wind loads, respectively, and the quality of conductors and insulators

Figure 1: Collapse of transmission steel towers during Wenchuan earthquake in China (2008).

was concentrated to arms or nodes of the finite element model.

Lin et al. [13] used the finite element software ABAQUS, to develop a subroutine based on the idea of the birth-death element to simulate the progressive collapse of transmission towers subjected to one-dimensional and three-dimensional earthquake, respectively. The weak parts of transmission towers were analyzed. They concluded that the transmission tower was more prone to collapsing under three-dimensional earthquake action. Three main methods can be used to analyze structural progressive collapse: theoretical analysis, experimental study, and numerical simulation. Given that the collapse process of structures involves many complicated nonlinear cases, theoretical analysis is difficult and cannot accurately evaluate the structural failure mechanisms. In addition, conducting structural collapse tests is expensive and dangerous, and the experimental process is difficult to control. Therefore, the numerical simulation method is widely adopted for the collapse process of structures. At present, the main methods of simulating structural collapse can be summarized as follows. (1) The finite element method (FEM): firstly, the structure is discretized according to the theory of the variational principle and continuum mechanics. Next, the element stiffness matrix of each discrete element is established. Then the global stiffness matrix is formed. Finally, the structural analysis is conducted by solving motion equations. If large deformation and nonlinear problems are involved, then the FEM can lead to the convergence problem of the numerical results. Thus, special treatment measures are needed to control the strong nonlinear behavior in the collapse process of structures. Other methods are needed to solve problems of discontinuity, such as those of fractures and collisions [14–16]. Numerical simulation of the collapse process of structures is usually based on explicit integration of the finite element program. Currently, some finite element software packages, such as LS-DYNA, ABAQUS/Explicit and MSC-MARC, can be used to simulate structural collapse. (2) The discrete element method (DEM): according to the Newtonian mechanics, the explicit time integration is adopted to solve governing equations and discontinuous problems involving the contact and collision between elements. In recent years, scholars have applied the DEM to simulate the structural collapse of brittle materials, such as concrete structures [17, 18]. However, the DEM is mainly used in the simulation of particulate materials. When the DEM is applied to simulate a large 3D space structure, the modeling process is more complicated and the analysis requires an excessively large amount of calculations; furthermore, the calculation results are also inaccurate. (3) The finite particle method (FPM): the FPM was proposed by Ting et al. [19, 20]. In space functions, the structure is discretized into finite number of particles connected to one another with a massless element. In time functions, the structural motion process is divided into a limited time element called the path element, in which motion equations can be established and solved by applying Newton's second law to each particle. Therefore, the entire structural mechanical behavior can be described by this method. As a particle method, it is possible to add or delete particles and elements in the FPM, which is important in the simulation of structural collapse. Particularly, no iterations are necessary to follow nonlinear laws, and no global matrices are formed.

The objective of this work is to establish a general finite particle method framework for simulating the collapse process of the transmission steel tower, including the discretization of the structure, motion equation of particles, the internal force calculation, and the explicit time integration and solution. This study conducts the collapse simulation of the transmission steel tower model based on the FPM. The three-dimensional finite particle model of transmission steel tower is developed in MATLAB. The static and elastic seismic response analysis of transmission tower is carried out and calculation results of the FPM agree well with those of the FEM, respectively. The failure criterion based on the ideal elastic-plastic model and the failure mode are proposed. Finally, the collapse simulation of the transmission steel towers subjected to unidirectional and three-dimensional earthquake ground motions can be successfully carried out using the finite particle method.

2. Description of Finite Particle Method

The FPM has three basic concepts: the point value description, the path element, and the virtual reversed movement. In space, the structure is discretized into certain number of particles by point value description. In time, the motion process is divided into certain number of periods through the path element. Moreover, the internal force of elements can

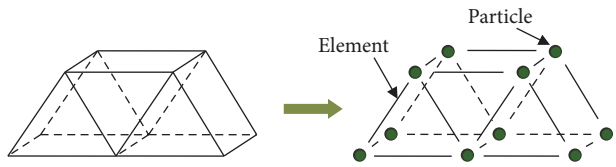

Figure 2: 3D truss structure and discretization in the FPM.

be calculated through virtual reversed movement. Finally, the mechanical behavior of structural systems can be accurately described by the FPM.

2.1. Discretization of the Truss Structure. Structural analysis is primarily used to study structural properties such as deformation, internal force, and displacement when structures are subjected to external action. The basic element of structure in the FPM is the particle, and the mass, space position, internal force, and deformation of the particle are described by the property of particle (Figure 2). However, elements are not used to describe the structure but to represent the topological relationship between two particles. And elements do not have mass, which is equivalent to the particles.

2.2. Establishment of Motion Equations for Truss Structure. The motion process of structures is the function of space and time. In the FPM, the motion process of particle is divided into certain number of motions in the small time step and particle simultaneously meets the control equations. Motion of particle in the small time step is called a path element, which is applied to simulate actual motion of structures. During the path element, the number and mass of particles in structural space, the connection, and mechanical properties of elements, the displacement constraints will remain unchanged. However, it can be changed only between path elements such as fracture, yield, and collision of structural members.

By the point value description and the path element, the structural motion in real time and space can be equivalent to the motion of particles at the small time step, and this motion follows Newton's second law. Therefore, the motion equation of particle in every path element can be established using Newton's second law. For space truss structures, the displacement of a particle can be decomposed into three translation degrees of freedom. In order to conduct the seismic response analysis using FPM, the acceleration time history record is imposed on particles of the upper structure. So, the motion equation of particles subjected to the earthquake can be expressed as

$$m\frac{d^2}{dt^2}\begin{bmatrix} d_x \\ d_y \\ d_z \end{bmatrix} = \begin{bmatrix} f_x^{\text{ext}} \\ f_y^{\text{ext}} \\ f_z^{\text{ext}} \end{bmatrix} + \begin{bmatrix} f_x^{\text{int}} \\ f_y^{\text{int}} \\ f_z^{\text{int}} \end{bmatrix} + \begin{bmatrix} f_x^{\text{damp}} \\ f_y^{\text{damp}} \\ f_z^{\text{damp}} \end{bmatrix} + \begin{bmatrix} f_x^{\text{eaq}} \\ f_y^{\text{eaq}} \\ f_z^{\text{eaq}} \end{bmatrix}, \tag{1}$$

where m is the equivalent mass of the particle, $[d_x \ d_y \ d_z]^T$ is the displacement vector of the particle, $F^{\text{ext}} = \left[f_x^{\text{ext}} \ f_y^{\text{ext}} \ f_z^{\text{ext}}\right]^T$ is the equivalent external force vector acting on the particle, $F^{\text{int}} = \left[f_x^{\text{int}} \ f_y^{\text{int}} \ f_z^{\text{int}}\right]^T$ is the equivalent internal force vector exerted by the elements connected with the particle, $F^{\text{damp}} = \left[f_x^{\text{damp}} \ f_y^{\text{damp}} \ f_z^{\text{damp}}\right]^T$ is the damping force, and $F^{\text{eaq}} = \left[f_x^{\text{eaq}} \ f_y^{\text{eaq}} \ f_z^{\text{eaq}}\right]^T$ is the earthquake action when structures are subjected to the earthquake ground motions.

In (1), the damping force is expressed as

$$\begin{bmatrix} f_x^{\text{damp}} \\ f_y^{\text{damp}} \\ f_z^{\text{damp}} \end{bmatrix} = -\mu m \begin{bmatrix} \dot{d}_x \\ \dot{d}_y \\ \dot{d}_z \end{bmatrix}, \tag{2}$$

where μ is damping factor which is the same as the definition in the dynamic relaxation method [21], and the structural damping is considered. $\left[\dot{d}_x \ \dot{d}_y \ \dot{d}_z\right]^T$ is the velocity vector of the particle.

The effect of earthquake action is similar to that of the external forces, and earthquake action can be calculated in

$$\begin{bmatrix} f_x^{\text{eaq}} \\ f_y^{\text{eaq}} \\ f_z^{\text{eaq}} \end{bmatrix} = -m \begin{bmatrix} \ddot{x}_{gx} \\ \ddot{x}_{gy} \\ \ddot{x}_{gz} \end{bmatrix}, \tag{3}$$

where $\left[\ddot{x}_{gx} \ \ddot{x}_{gy} \ \ddot{x}_{gz}\right]^T$ is the three-dimensional earthquake ground acceleration.

2.3. Internal Force Calculation of the Bar Element. The relationship between the internal force of elements and particle position should be solved in order to accurately depict structural deformation. However, the internal force of the bar element is only related to pure deformation in the relative position. In the FPM, virtual reversed movement is utilized to calculate internal forces of bar elements. Because the internal forces (axial force) are related only to the deformation of the bar element, it is necessary to remove rigid body translations and rotations from the relative displacement. The path element assumes that the bar element has virtual reversed translations and virtual reversed rotations to obtain its pure deformation (Figure 3).

The time segment is assumed to be very small, and the deformation during the time step is infinitesimal. So, the engineering stress and strain could be used to calculate the

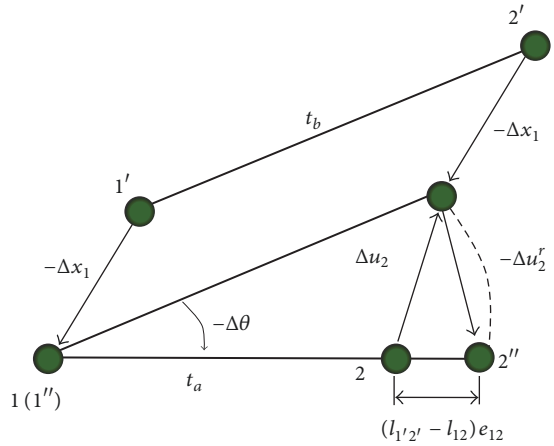

Figure 3: Reversed translation and rotation.

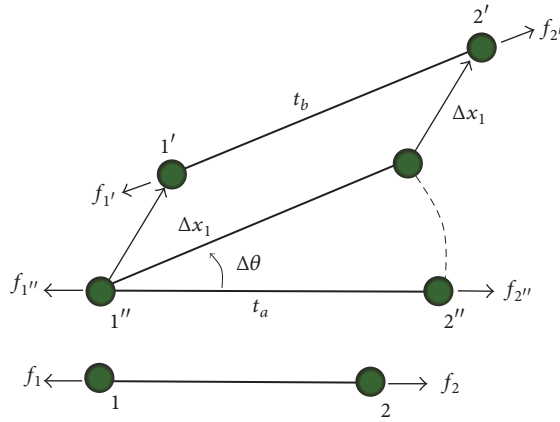

Figure 4: Particle internal force.

internal forces of truss bars [22]. As the bar element, its deformation is only related to the variation of the bar length, and the incremental deformation of the bar can be obtained.

$$\Delta u_2^d = (l_{1'2'} - l_{12})\, e_{12}, \tag{4}$$

where l_{12} and $l_{1'2'}$ are the length of element 1-2 at time t_a and t_b, respectively, and e_{12} is directional vector of element at time t_a.

The internal force (axial force) of bar element can be expressed as

$$f_{2''} = f + \Delta f = \left[\sigma A + \frac{EA}{l_{12}}(l_{1'2'} - l_{12})\right] e_{12}, \tag{5}$$

where f and σ are axial force and axial stress of bar element 1-2 at time t_a, respectively; Δf is the incremental axial force of bar element 1-2 at time t_b; E and A are Young's modulus and the section area of bar element 1-2, respectively.

According to the static equilibrium condition

$$f_{1''} = -f_{2''}. \tag{6}$$

When the axial force at the virtual position $1''$-$2''$ has been obtained, let the bar element is imposed a rotation $\Delta\theta$ and a translation Δx_1 to return to its original position (Figure 4). In the process, only the direction of element axial force is changed, and the internal force of the bar element can be determined from

$$f_{2'} = -f_{1'} = \left[\sigma A + \frac{EA}{l_{12}}(l_{1'2'} - l_{12})\right] e_{1'2'}, \tag{7}$$

where $f_{1'}$ and $f_{2'}$ are the internal forces of the particles $1'$ and $2'$, respectively.

Finally, the internal force of the particle can be obtained by the summation of all axial forces of bar elements connected to it.

2.4. Solution of Particles Motion Equation. The implicit time integration solution of motion equations requires iterations, so the calculation process is complex and there may be no convergence problem. In the FPM, explicit time integration is adopted to solve the motion equation particles. The advantages of explicit time integration lie in having a concise formula and requiring no iterations.

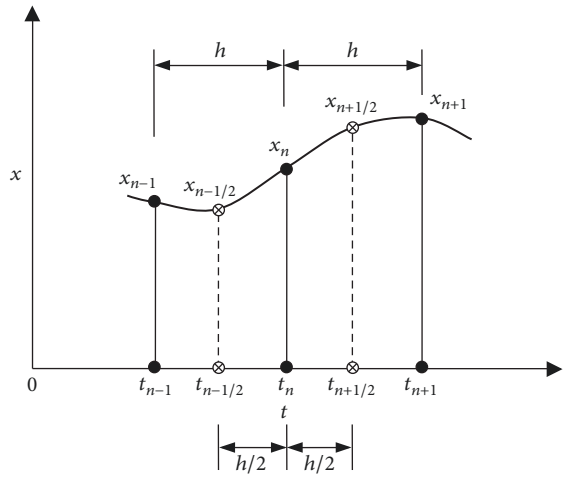

Figure 5: Central difference method.

According to the central difference method (Figure 5), the velocity of the particle dx_n/dt and the acceleration of the particle d^2x_n/dt^2 can be expressed as

$$\frac{dx_n}{dt} = \frac{1}{2h}\left(x_{n+1} - x_{n-1}\right),$$
$$\frac{d^2x_n}{dt^2} = \frac{1}{2\left((1/2)h\right)}\left(\frac{d}{dt}x_{n+1/2} - \frac{d}{dt}x_{n-1/2}\right) \quad (8)$$
$$= \frac{1}{h^2}\left(x_{n+1} - 2x_n + x_{n-1}\right).$$

Substituting (9) into (1), the difference calculation formula of particles under earthquake ground motions can be obtained as follows:

$$x_{n+1} = 2x_n - x_{n-1} + \frac{F^{\text{ext}} + F^{\text{int}} + F^{\text{damp}} + F^{\text{eaq}}}{m}h^2. \quad (9)$$

Thus, difference calculation can be started from $n = 1$ in a step-by-step manner using (9), and the corresponding displacement of particles of the structure can be solved in every time step; finally, structural behavior can be described.

2.5. Calculation Procedures. The calculation procedure of truss structures using the FPM is illustrated in the following steps.

Step 1. At the first time step, $t = 0$, the structure is dispersed into finite particles, the initial conditions of the structural calculation are determined, and the topological relationship between particles is defined, which is called as the connection of elements.

Step 2. When $n = 0$, calculate the one step displacement value x_{-1} before initial displacement of each particle according to (5).

Step 3. At any time step, $n \neq 0$, update the position of all particles, define special constraint points, and start the forward recursive calculation.

Step 4. Update internal and external forces of particles based on the new particle position.

Step 5. Define special constraint particles according to the boundary condition of the structure.

Step 6. Determine whether t_n is the finial time step, and compare t_n with total calculation time. If t_n is less than the total time, then repeat Steps 3–6. Otherwise, end the process.

Step 7. Conduct postprocess. Obtain the required results.

The calculation flow chart of the truss structure using the FPM is shown in Figure 6.

2.6. Failure Criterion and Failure Mode of Members. The collapse of structures is caused by the destruction of the material. It is necessary to define the failure criterion of material when simulating the collapse process of truss structures, the conditions must be confirmed when the material reaches the ultimate strength and members' damage. At the same time, the failure mode considering the destroyed behavior must be defined, and collapse analysis of truss structures can be conducted by defining the failure criterion and failure mode of members.

2.6.1. Failure Criterion. The main objective of this paper is to simulate the collapse process of transmission tower, which is a macroscopic process of spatial structural motion. However, the accurate fracture criterion of spatial steel structure is related to the research of fracture mechanics and structural material testing, which makes the problem too complicated. Thus, the spatial bar element in the FPM is simplified as the circular section without considering the emergence and development of cracks when material failure occurs. Therefore, the spatial bar element in steel structures is regarded as the ideal element that has no initial defects, and failure directly occurs when this failure reaches the stress-strain limit. There are three kinds of failure rule for 3D

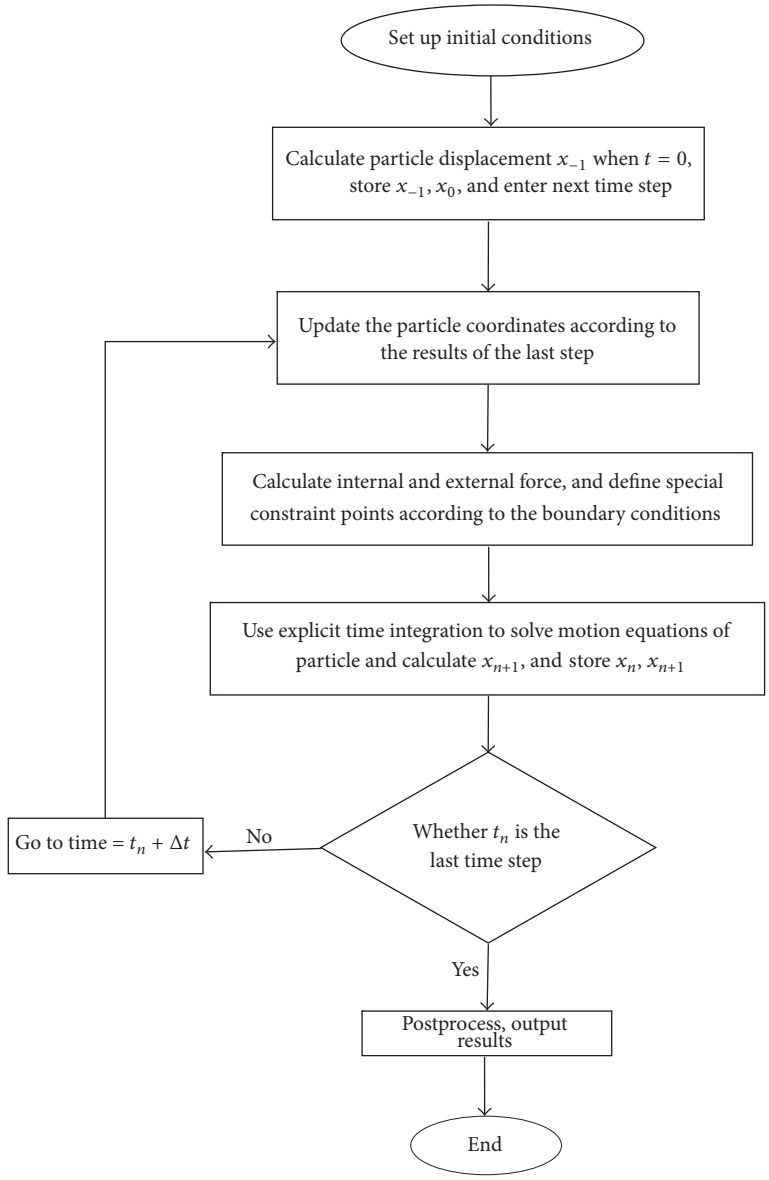

Figure 6: Calculation flow chart using the FPM.

truss element, that is, strength failure rule, ultimate strain failure rule, and compression member buckling and softening failure rule. Strength failure rule is suitable to the hard brittle member, ultimate strain failure rule applies to the member with smaller slenderness and good ductility, and compression member buckling and softening failure rule can account for several failure modes of the larger slenderness member [23]. In this paper, the ultimate strain failure will be adopted as shown in Figure 7. The relationship between stress and strain is linear until the member axial tensile or compressive stress reaches the yield stress value of the material σ_{crit}. Then, the material behavior is proposed to be plastic until failure happens. However, the exact critical strain value at the point at which failure happens is not quite clear. According to several experiments, the critical axial tensile value is suggested to be approximately three times the yield strain, $\varepsilon_{\text{crit}} = 3\varepsilon_y$ [24]. After failure happens, the fracture member may have one or two free ends. If the external force is not exerted, unloading will occur in the failure member. The unloading is elastic in nature with the same slope as the initial loading phase.

2.6.2. Failure Mode. Fracture behaviors of members involve a series of problems, such as the separation of particles, the redistribution of internal forces and masses, and the redefinition of topological relations of elements [25]. In order to simulate these behaviors in the analysis of the FPM, it is necessary to establish the fracture failure model. When the stress reaches the failure criterion of the material, the failure mode of members may be separated from the two ends of the particle simultaneously, and it is also possible to be separated from one side of the particle. Particles

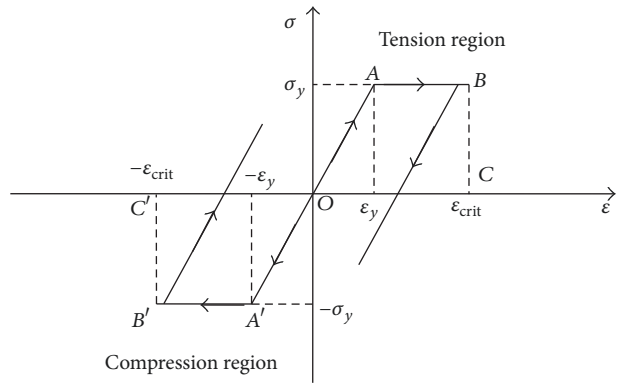

Figure 7: Ideal elastic-plastic stress-strain curve of steel.

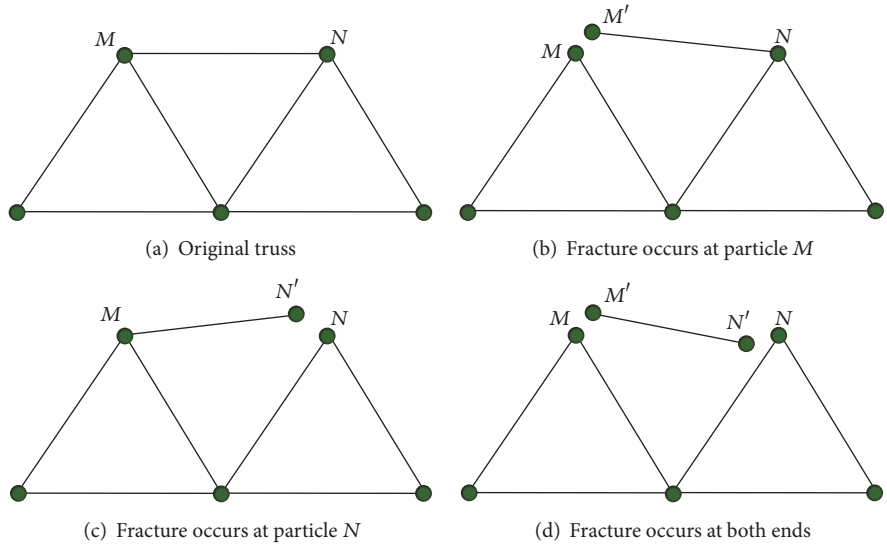

(a) Original truss (b) Fracture occurs at particle M

(c) Fracture occurs at particle N (d) Fracture occurs at both ends

Figure 8: Failure modes of members of the truss.

maintain a dynamic balance under internal and external forces. Although axial forces at the both ends of the bar element are the same, the resultant forces of particles at the both sides of the bar element will not necessarily be the same. Thus, the resultant forces of particles at the both sides of the bar element are needed to be compared, and the fracture of members will occur at the end of greater resultant forces of particles. $|f_M|$ and $|f_N|$ are defined to resultant forces of particles at M end and N end of the bar element, respectively (Figure 8(a)). If $|f_M| > |f_N|$, the fracture of the member occurs at particle M, the new particle M' is generated and the element is connected to the new particle M' as shown in Figure 8(b). If $|f_M| < |f_N|$, the fracture of the member occurs at particle N, the new particle N' is generated, and the element is connected to the new particle N' as shown in Figure 8(c). If $|f_M| = |f_N|$, the fracture of the member happens at both ends of the member, then two new particles M' and N' are generated simultaneously, and the element is connected to the new particles M' and N'. Finally, the element is completely separated from the structure as shown in Figure 8(d).

2.7. Example Analysis. To verify the capabilities of the computation code, two examples are designed: Example 1: buckling analysis of 24-bar star dome; Example 2: elastic-plastic loading of three-bar plane truss.

Example 1 (buckling analysis of 24-bar star dome). This example is analyzed using FPM, and the results are compared with the nonlinear finite element method. The space truss element is adopted, and the top center node is subjected to the concentrated force F_P in the Z direction (as shown in Figure 9), elastic modulus $E = 3.03 \times 10^3$ MPa, cross-sectional area $A = 317\,\text{mm}^2$, and time step $\Delta t = 1 \times 10^{-3}$ s. Displacement control is used in the analysis, and the displacement step $\Delta d = 1 \times 10^{-4}$ mm.

The Z-direction displacement of node 1 and node 2 is tracked. The load-displacement curves are shown in Figures 10(a) and 10(b), respectively, and the results are in good agreement with the reference [26]. It is shown that the buckling analysis of the structure using the finite particle method is feasible.

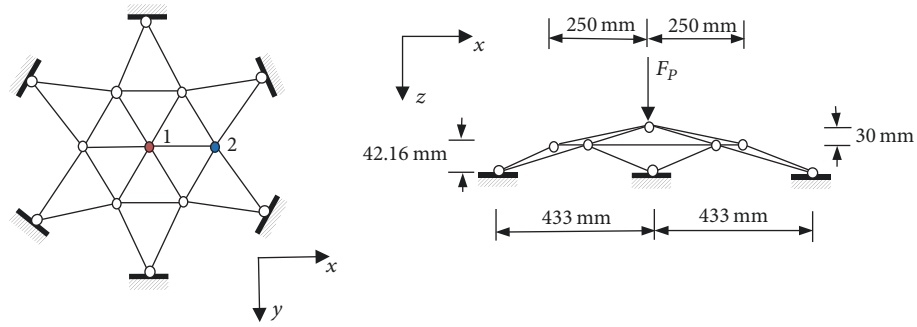

FIGURE 9: 24-bar star dome geometry and loading.

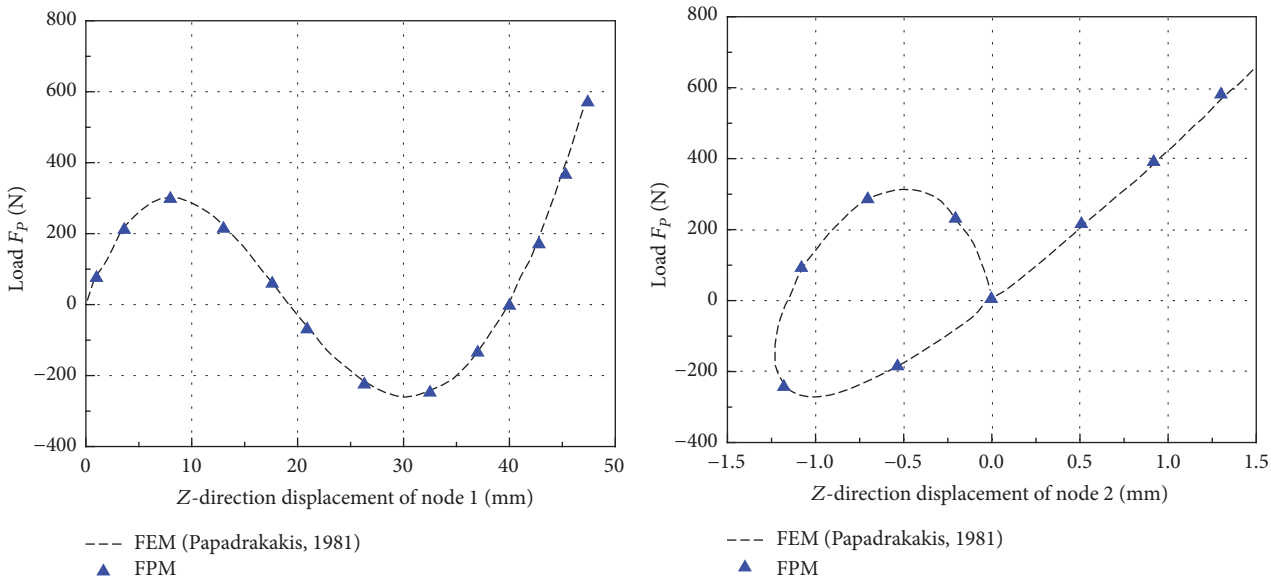

(a) Node 1 (b) Node 2

FIGURE 10: Load-displacement curves of node 1 and node 2 in the Z direction.

Example 2 (elastic-plastic loading of three-bar plane truss). The three-bar plane truss is subjected to the load F_P in the y direction (shown in Figure 11), the cross-sectional area of bars is A, elastic modulus at the elastic phase is E, yield strength is σ_y, the length of BD bar is l, and AD = CD.

Using the ideal elastic-plastic model, the theoretical solution of the load-displacement at point D is expressed as follows:

$$\text{When } F_P \le F_{Pe} \quad F_P = \frac{EA\left(1 + 2\cos^3\theta\right)\Delta}{l}, \tag{10}$$

$$\text{When } F_{Pe} < F_P \le F_{Py} \quad F_P = \sigma_y A + \frac{2EA\left(\cos^3\theta\right)\Delta}{l}, \tag{11}$$

$$\text{When } F_P > F_{Py} \quad F_P = F_{Py}, \tag{12}$$

where $F_{Pe} = \sigma_y A(1 + 2\cos^3\theta)$ and $F_{Py} = \sigma_y A(1 + 2\cos\theta)$.

The analysis is conducted using the finite particle method, elastic modulus value at the elastic phase is $E = 206\,\text{GPA}$, yield strength value is $\sigma_y = 235\,\text{MPa}$, the length of BC bar $l = 1\,\text{m}$, density is $\rho = 7850\,\text{kg/m}^3$, $\theta = 45^\circ$, and time step is $\Delta t = 1 \times 10^{-5}\,\text{s}$. The truss structure is subjected to the slow load action, and the results are turned into the dimensionless curve and compared with the theoretical solution as shown in Figure 12.

As can be seen from Figure 12, when $\theta = 45^\circ$ and $\Delta_y/\Delta_e = 2$, $F_{Py}/F_{Pe} = 1.41$. FPM analysis results are very close to the theoretical solution. However, the FPM result of the load-displacement curve is slightly higher than that of the theoretical solution when the bars go into the plastic stage. The reason is that the structure is continuously loaded in the actual analysis, and even if there is a small load increment, the great strain will be produced in the truss structure. But the theoretical solution does not consider the full plastic loading, and this small difference is considered to be reasonable. Simultaneously, the numerical examples show that the finite particle method can effectively simulate the elastic-plastic properties of truss structures.

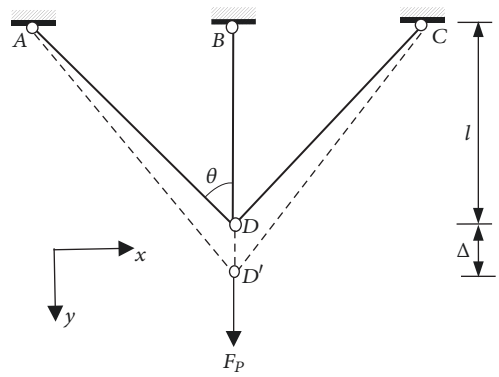

Figure 11: Three-bar plane truss.

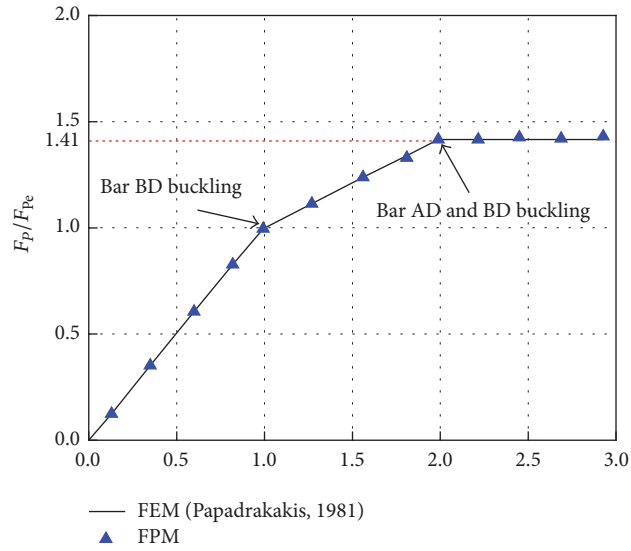

Figure 12: Load-displacement curve.

3. Establishment and Verification of Transmission Tower Model

3.1. Establishment of the Model of Transmission Steel Tower. A 110 kV double-circuit linear transmission tower structure is studied. The elevation drawing of transmission tower is shown in Figure 13. The total height of the transmission tower is 21 meters, the sections of tower columns are square, and materials are equilateral angle steel (Table 1). Software ANSYS and software MATLAB are used to establish the model of the transmission tower structure by the FEM and the FPM, respectively. Although ANSYS is widely used and is relatively mature finite element software, the study on finite particle method has just started by the MATLAB program. To verify the accuracy of the model of the FPM, the finite element model of the transmission tower is also established by ANSYS.

On one hand, the finite element model is established in ANSYS by adopting the element beam 188 in Figure 14, cross section of the elements is L-shaped equilateral steel angle, and the rigid joint of beam elements is assumed without considering eccentric connections. The finite element model has 522 elements and 172 nodes. On the other hand, a finite particle model of transmission tower is established by adopting the truss element in which only the axial force is considered. So, each particle has only three translation degrees of freedom in the directions of x, y, and z; thus, all joint connections that can be regarded as hinges and elements in the FPM were modeled by bar elements. During the modeling of the transmission tower, the node coordinates, connections, and section parameters of elements are derived directly from the ANSYS model and then imported into the compiled MATLAB program. When the initial parameters of the analysis are inputted, the finite particle model is established in MATLAB as shown in Figure 15. The number of elements and nodes in the FPM is the same as that of the FEM, that is, 522 elements and 172 nodes. In the FPM, the section area of the bar element is only considered and the shape of bar element is not considered.

3.2. Static Analysis and Verification of the Transmission Tower. The static analysis of the transmission tower is conducted using the FEM (in ANSYS) and FPM (in MATLAB), respectively. The calculation results were compared in order to verify the correctness of the finite particle model. Three kinds of static loads are applied, respectively. (1) The vertical load

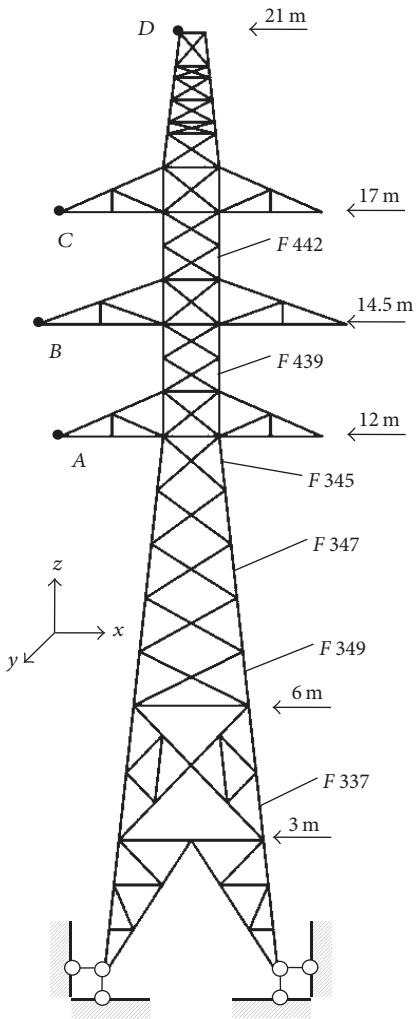

Figure 13: Elevation of the transmission tower.

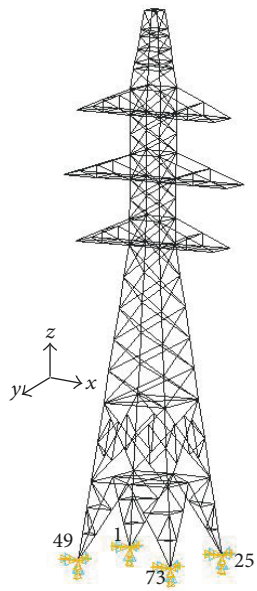

Figure 14: FEM model (ANSYS).

Table 1: Material parameters of transmission tower.

Number	Material type	Section area /m^2	Density /kg·m^{-3}	Elastic modulus /Pa	Member type
(1)	$L100 \times 10$	$1.93E-03$	$7.80E+03$	$2.06E+11$	Main material
(2)	$L50 \times 4$	$3.90E-04$	$7.80E+03$	$2.06E+11$	Auxiliary material
(3)	$L40 \times 3$	$2.36E-04$	$7.80E+03$	$2.06E+11$	Diagonal brace
(4)	$L90 \times 8$	$1.39E-03$	$7.80E+03$	$2.06E+11$	Main material
(5)	$L45 \times 4$	$3.49E-04$	$7.80E+03$	$2.06E+11$	Auxiliary material
(6)	$L63 \times 5$	$6.14E-04$	$7.80E+03$	$2.06E+11$	Main material
(7)	$L80 \times 7$	$1.09E-03$	$7.80E+03$	$2.06E+11$	Main material

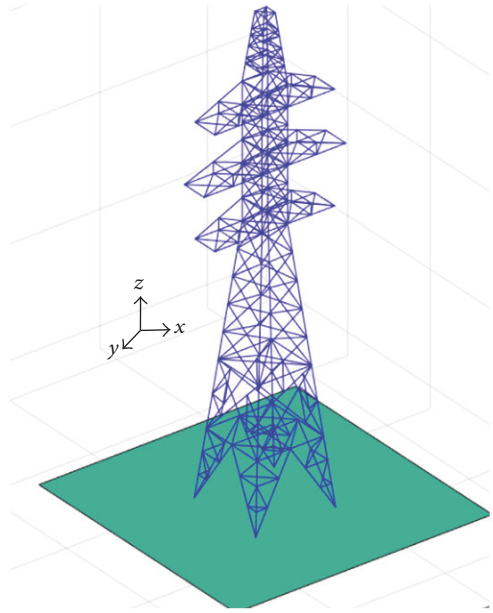

Figure 15: FPM model (MATLAB).

$F = -1000N$ is imposed on the four corners of the tower in the z-direction of the model. (2) The transverse load $F = 200N$ is applied at four corners of the tower in the x-direction of the model. (3) The gravity load is applied for the entire structure. The acceleration of gravity is $g = 9.8\,\text{m/s}^2$. The analysis results are compared by using ANSYS and MATLAB when the structure is imposed on three kinds of static loads (Tables 2, 3, and 4). Table 2, Table 3, and Table 4 show the results, including the support reactions of the four supports (in Figure 11) and the corresponding displacements of four nodes A, B, C, and D at different heights (in Figure 10).

Tables 2, 3, and 4 show that the relative errors of support reactions are small under three kind of loads, all of them are no greater than 1%, and the relative deviation is only 0.06% under vertical load. Thus, this means that the finite particle method is very accurate in calculating the support reactions of the transmission tower. By comparison of the FEM and the FPM, relative deviations of displacement of the tower are less than 3% under vertical and transverse loads, respectively. It indicates that the lateral stiffness of the FPM model is very close to the FEM model. Because the global stiffness matrix is not assembled in the FPM, the dynamic characteristics of the tower can be obtained. In addition, the maximum relative deviation of displacements of the tower which is 4.11% under the gravity load caused by the distribution pattern of the mass in these two methods is different. In the FPM, the mass is concentrated on particles which are equivalent to the concentrated load at the node. However, in the FEM, mass is considered based on the distribution of the actual mass which is equivalent to the uniform loads on bar elements. In conclusion, the results of the static analysis of the finite particle method are consistent with that of the finite element method, and the accuracy of the model of the finite particle method is validated for the following application in seismic response analysis and the collapse simulation of the transmission tower.

3.3. Linear Seismic Response and Verification of the Transmission Steel Tower. The acceleration time history of El Centro earthquake ground motion record (NS) is selected to conduct

Table 2: Support reactions and vertical displacements of nodes under vertical loads.

Methods	Vertical support reactions/N				Vertical displacements/mm			
	Support point 1	Support point 25	Support point 49	Support point 73	Node A	Node B	Node C	Node D
FEM	967.8	999.3	999.3	1033.6	−0.0359	−0.0422	−0.0528	−0.0973
FPM	968.4	999.9	999.9	1031.8	−0.0367	−0.0427	−0.0540	−0.0990
Relative deviation	0.06%	0.06%	0.06%	−0.17%	2.17%	1.23%	2.24%	1.80%

Table 3: Support reactions and horizontal displacements of nodes under horizontal loads.

Methods	Transverse support reactions/N				Transverse displacements/mm			
	Support point 1	Support point 25	Support point 49	Support point 73	Node A	Node B	Node C	Node D
FEM	−198.8	−198.2	−201.6	−201.4	0.340	0.655	1.068	1.916
FPM	−197.2	−197.2	−202.8	−202.8	0.349	0.672	1.094	1.957
Relative deviation	−0.80%	−0.50%	0.60%	0.70%	2.65%	2.60%	2.34%	2.14%

Table 4: Support reactions and vertical displacements of nodes under gravity loads.

Methods	Vertical support reactions/N				Vertical displacements/mm			
	Support point 1	Support point 25	Support point 49	Support point 73	Node A	Node B	Node C	Node D
FEM	5637.4	5640.0	5635.9	5652.9	0.197	0.233	0.219	0.172
FPM	5651.7	5660.4	5656.2	5665.0	0.204	0.242	0.228	0.179
Relative deviation	0.25%	0.36%	0.36%	0.21%	3.55%	3.86%	4.11%	4.07%

the seismic response analysis. The peak ground acceleration (PGA) is adjusted to 1 m/s^2, and the time step of El Centro ground motion in the FEM is 0.02 s while the time step is 0.0001 s in the FPM by using linear interpolation method, and earthquake acceleration is inputted in the direction of transverse line direction of the transmission tower. Then the elastic seismic response analysis is carried out using FEM and FPM, respectively. The time history curves of the displacement of the particle at the top of the transmission tower by the two methods are shown in Figure 16.

Figure 16 shows that the results of the finite element method and the finite particle method to calculate the displacement response of the transmission tower under earthquake acceleration are very close and the maximum displacement is 5.28 mm in 4.96 s for the ANSYS analysis while that is 5.61 mm in 5.10 s for the MATLAB program. Thus, the relative error of displacement of particles is very small so that the time history of displacement is consistent.

Table 5 shows the maximum and minimal axial forces of some members of the transmission tower which are obtained by the FEM and the FPM. The axial forces calculated by the FEM are in good agreement with those by the FPM, and relative error is also within 5%. The seismic response analysis of the transmission tower is conducted by the FEM and the FPM using the same earthquake ground motion record, respectively. Results show that the time history of displacement maximum displacements and extreme value of axial forces are very close. These results also illustrated that the input method of the earthquake wave in the FPM is reliable. Therefore, the FPM can be applied to simulate the collapse analysis of the transmission tower by the MATLAB program.

4. Collapse Analysis of the Transmission Tower

4.1. Collapse Analysis under Different PGAs. When the collapse analysis of the transmission tower is carried out the effect of gravity is considered, the value of the virtual damping factor is set to 5, and the yield strength of material is 235 MPa. There are 522 elements in the finite particle model by MATLAB. According to "Code for Design of Steel Structures" [25], the stability factor of the member related to its slenderness ratio can be obtained. To simplify the analysis process, the stability factor φ of all members is set as 0.88. The first 10 seconds of acceleration time history of the El Centro earthquake ground motion record is selected. In order to study the collapse of the structure under different seismic PGA and determine the critical PGA of collapsed, the PGA value of the earthquake ground motion record is adjusted to 18 m/s^2, 20 m/s^2, 22 m/s^2, 24 m/s^2, and 26 m/s^2. Failure time of transmission tower structure and members can be obtained, such as the first member, 20% members of the structure, and the complete structure, and the results are listed in Table 6.

When PGA is 18 m/s^2, the structure does not destroy, and the elastic behavior occurs. The structure collapsed when PGA is greater than 18 m/s^2, and greater PGA values lead to earlier occurrences of collapse. According to the first damaged members, failure occurred at the 12 m height of the transmission tower when PGA is 20 m/s^2 and 22 m/s^2, respectively, whereas failure occurred at 6 m under 22 m/s^2 and 24 m/s^2. The damage location of the transmission tower will be different under different PGA values; namely, the destruction form is not the same. Because the space structure is very complex, no unified quantitative index to judge complete collapse of structure has been recorded. This paper uses the method in reference [22], which supposed that the structure completely collapsed when 20% of total members damaged. With the increase of the PGA, the time from first damage to complete collapse becomes much shorter. Furthermore, the time under the PGA for 22 and 24 m/s^2 is shorter than the time under 20 and 22 m/s^2, indicating a decrease of one order of magnitude. The greater PGA is, the quicker the structure collapses.

Failure modes under the PGA for 20, 22, 24, and 26 m/s^2 are shown in Figure 17. When PGA was 20 m/s^2, damage occurred mainly at heights of 6 and 12 m; when PG is 22 m/s^2,

Table 5: Maximum and minimal axial force of some members of tower.

Element number	F337	F349	F347	F345	F439	F442
Maximum (FEM)	−12816.4	−12665.6	−11463.9	−9838.9	−7166.8	−3151.7
Maximum (FPM)	−12556.6	−12263.6	−10982.1	−9481.6	−6946.7	−3133.3
Relative deviation	−2.03%	−3.17%	−4.20%	−3.63%	−3.07%	−0.59%
Minimum (FEM)	4222.9	4660.6	4658.9	4398.2	2901.7	842.0
Minimum (FPM)	4138.6	4471.3	4451.1	4292.2	2861.1	830.0
Relative deviation	−2.00%	−4.06%	−4.46%	−2.41%	−1.40%	−1.42%

Table 6: Failure time of the transmission tower subjected to different PGAs.

PGA/m·s^{-2}	18	20	22	24	26
First damaged time/s	No damage	6.76	5.92	5.66	4.93
Element number	No damage	138	139	359	349
Damaged time for 20% of members/s	No damage	8.34	6.97	5.85	5.06
Time from first crack to collapse/s	No damage	1.57	1.05	0.18	0.13

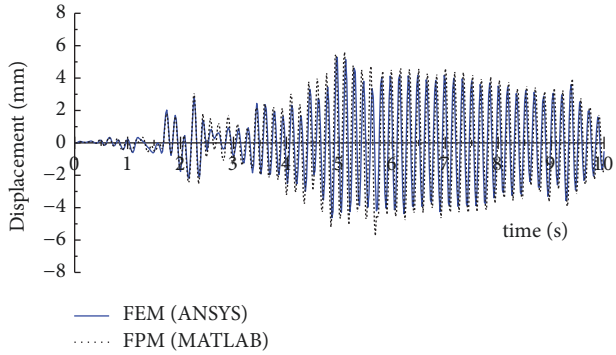

Figure 16: Time history curves of displacement of node D at the top of the transmission tower.

failure occurred at supports and the height of 6 and 12 m; when PGA reaches 24 m/s^2, failure occurs from the bottom to 14 m high; when PGA is 26 m/s^2, structural damage occurs at almost every height. Thus, when the PGA is large, the damage occurred early and the failure mode becomes massive.

4.2. Collapse Analysis under Unidirectional Earthquake Action. According to the discussion in the previous section, the critical PGA wherein the transmission tower started to collapse is between 18 and 20 m/s^2. With the increase of the PGA, collapse becomes severe and the duration of the process of collapse was abrupt. The PGA for 20 m/s^2 is selected to capture the details of the process of collapse more clearly. The process of transmission tower collapse is complex and involves a variety of nonlinear problems and fractures of materials as well as contact-impact problems. Contact-impact problems are a new research topic that is cumbersome to discuss; hence, this subject is not discussed. Only contacts between members and the ground are considered, which are simplified by using a simple spring model for simulation. Impacts, either among members or between members and structures, are not considered after fracture. The transmission tower starts to fail at $t = 6.76$ s and collapsed totally at $t = 8.34$ s, at which point the duration of the collapse is 1.57 s. The process of failure is simulated by using the FPM, and structural forms in every moment are captured. Elevation drawings of structural deformation are intercepted in several representative moments, as shown in Figure 18.

At $t = 6.9$ s, the fracture of elements firstly happen at the height of 12 m at $t = 7.0$ s; elements are subsequently destroyed at 6 m. Damage at these two heights is the main reason for the collapse of the transmission tower. At $t = 7.3$ s, destruction continues to worsen and elements of the transmission tower foot begin to damage. At $t = 7.6$ s, elements of the transmission tower at 17 m start to fail. Finally, the structural collapse processes continue at $t = 8.0$ s, and structure damage begins to worsen until the complete structural collapse appears due to gravity.

The transmission tower belongs to the statically indeterminate structures which possess many redundant constraints. Redundant constraints are considered to prevent the progressive collapse of the structure. However, for the transmission tower truss structure, the redistribution of internal forces

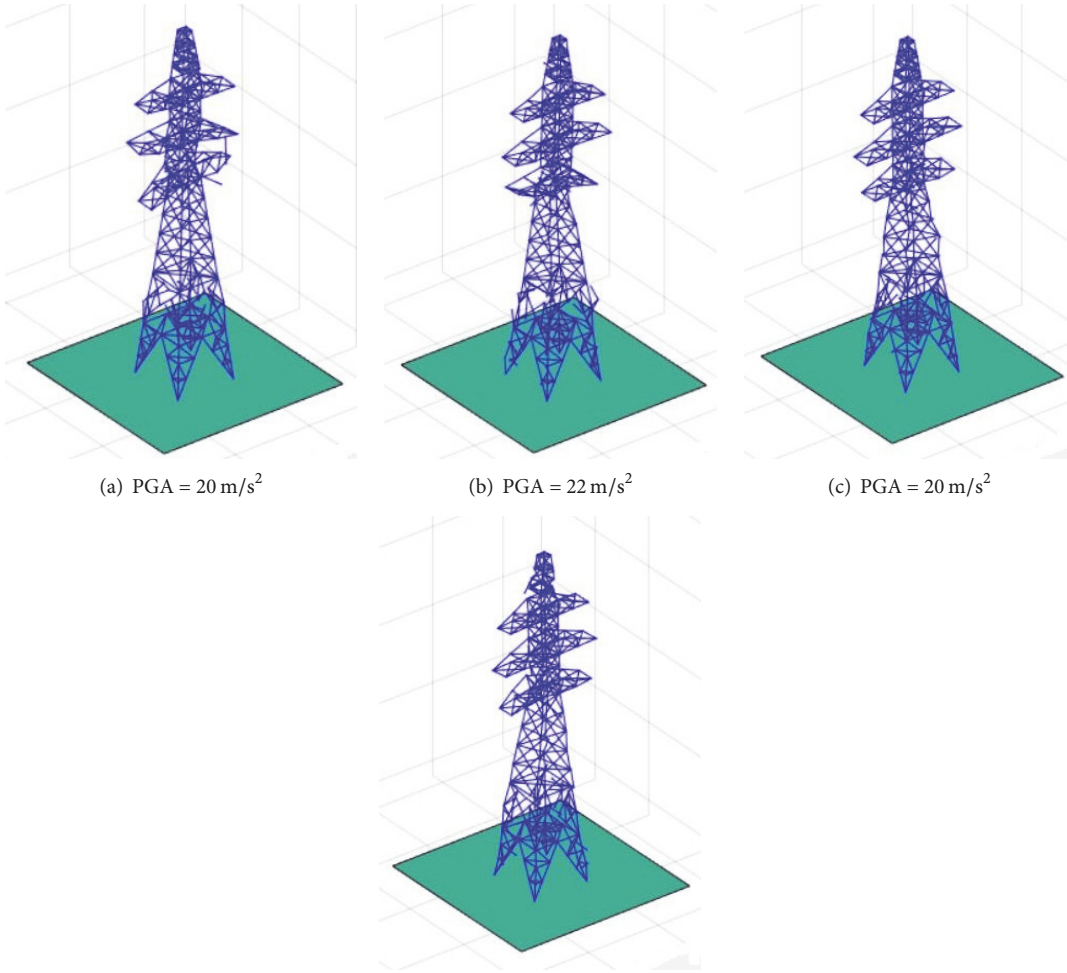

(a) PGA = 20 m/s^2 (b) PGA = 22 m/s^2 (c) PGA = 20 m/s^2

(d) PGA = 22 m/s^2

Figure 17: Damage drawing of the transmission tower under different PGAs.

will occur if a bar element is damaged. This redistribution will lead to the destruction of other elements, and the structure will present mechanism failure until it is eventually collapsing.

Some axial force responses of representative elements are extracted for a more intuitive understanding of the collapsing process of the transmission tower, as shown in Figure 19. For example, element 139 is the bar that is first cracked, in which the failure mode is buckling under compression and simultaneously breaks off at both ends of the bar element. Before the fracture, the axial force changed with the change of earthquake acceleration. At about $t = 6.7$ s, the element becomes a free element and the axial force gradually decreases due to damping energy dissipation. In addition, tensile failure first happens for element 137, and the fracture also happened at $t = 6.7$ s. Two cases are available to define the failure mode of the fracture: the fracture occurring at both ends simultaneously and a fracture occurring as just one end of the element. Element 137 belongs to the latter. Before damage, the axial force changed with the change of earthquake acceleration. Moreover, after damage, one end of the bar became free whereas another remains connected to the remaining structure. The axial forces irregularly change under earthquake ground motions.

4.3. Collapse Seismic Fragility Analysis. Seismic fragility in structural engineering is the relationship between ground motion intensity measure (IM) and structural damage. The probability of exceeding a damage state under a given ground motion can be quantitatively described by the fragility curve. The calculation method can be divided into parameter analysis method and nonparametric analysis method [27]. The difference between the two approaches is whether the probability distribution of engineering demand parameters (EDP) needs to be assumed in advance. Nonparametric analysis does not need to assume the probability distribution of EDP. By setting different IM levels, a large number of nonlinear time history analyses are conducted to calculate the failure probability of the structure in different damage states. When selecting EDP, the relevant performance parameters (such as force, displacement, velocity, acceleration, energy, and damage) are used to describe the

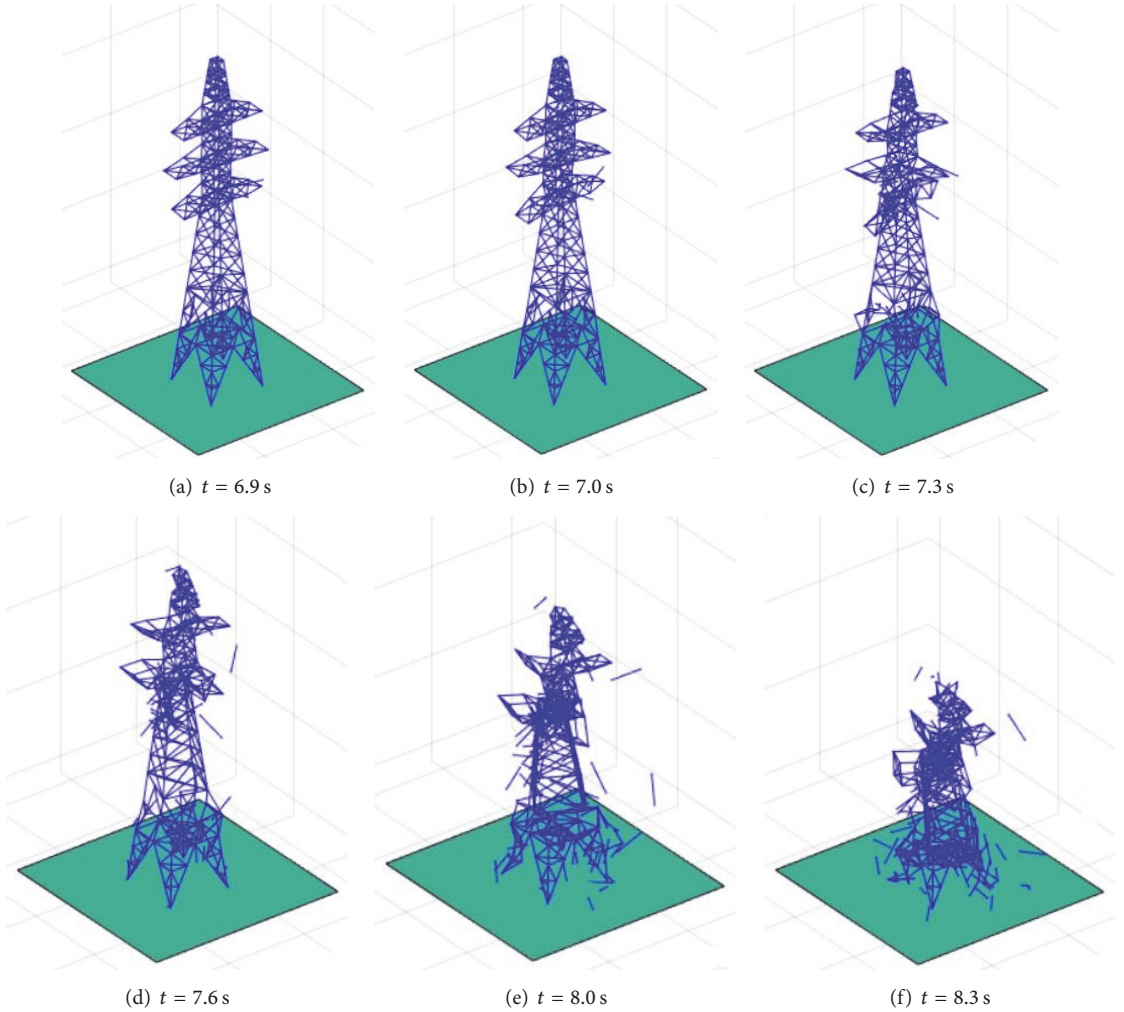

(a) $t = 6.9$ s (b) $t = 7.0$ s (c) $t = 7.3$ s

(d) $t = 7.6$ s (e) $t = 8.0$ s (f) $t = 8.3$ s

Figure 18: Failure process of the transmission tower at different time.

strength degradation, stiffness degradation, damage state, and ductility of the structure under earthquake action. Displacement is easy to apply and quantitatively describe the ultimate state of the structure under earthquake action [28]. In this paper, the maximum horizontal top displacement of the transmission tower $u_{\max}$ is selected as EDP. Combined with Chinese code, the top displacement of the tower should not exceed $3h/1000$ (h is the tower height) to ensure that the transmission steel tower is in serviceability limit states. Top displacement should not exceed $h/80$ to ensure that the transmission steel tower does not collapse [29].

(1) Parameter Analysis Method. For the performance-based seismic evaluation of the transmission tower, the structural earthquake collapse fragility analysis is defined as the conditional probability of the collapse of the structure under given earthquake intensity measure. The mathematical expression is

$$P_f = P\left(\text{Collapse} \mid \text{IM} = \text{im}\right), \tag{13}$$

where P_f is structural collapse probability, IM is the ground motion intensity measure, and PGA is taken as IM in this paper.

It is assumed that the PGA value of the structure collapses from the lognormal distribution; the probability of the collapse of the structure under a given PGA can be expressed as follows:

$$P_f = \Phi\left(\frac{\ln \text{PGA} - \widehat{\mu}_{\ln \text{PGA}|\text{Collapse}}}{\widehat{\sigma}_{\ln \text{PGA}|\text{Collapse}}}\right), \tag{14}$$

where $\Phi(\cdot)$ is the standard normal distribution function and $\widehat{\mu}_{\ln \text{PGA}|\text{Collapse}}$ and $\widehat{\sigma}_{\ln \text{PGA}|\text{Collapse}}$ are the mean and standard deviation of $\ln \text{PGA}_i$ for structural collapse, which can be calculated as follows, respectively:

$$\widehat{\mu}_{\ln \text{PGA}|\text{Collapse}} = \ln\left(\frac{\widehat{\mu}_{\text{PGA}|\text{Collapse}}}{\sqrt{\delta^2 + 1}}\right),$$

$$\widehat{\sigma}_{\ln \text{PGA}|\text{Collapse}} = \sqrt{\ln\left(\delta^2 + 1\right)},$$

Table 7: Characteristics of the earthquake ground motion records.

Number	Earthquake	Year	Magnitude	Station	PGA (g)
(1)	Imperial valley	1951	5.6	EI Centro-9	0.0294
(2)	Hollister	1961	5.6	Hollister City Hall	0.1210
(3)	Imperial valley-06	1979	6.53	Parachute Test Site	0.1661
(4)	Imperial valley-06	1979	6.53	Plaster City	0.0501
(5)	Loma Prieta	1989	6.9	Capitola	0.4803
(6)	Loma Prieta	1989	6.93	Coyote Lake Dam (Downst)	0.1718
(7)	Northridge-01	1994	6.69	Arcadia-Arcadia Av	0.0951
(8)	Kobe, Japan	1995	6.90	Abeno	0.2219
(9)	Kobe, Japan	1995	6.90	Amagasaki	0.3011
(10)	Kobe, Japan	1995	6.90	Fukushima	0.0337
(11)	Chi-Chi, Taiwan	1999	7.62	CHY047	0.1825
(12)	Chi-Chi, Taiwan	1999	7.62	CHY088	0.1796

$$\delta = \frac{\widehat{\sigma}_{\mathrm{PGA|Collapse}}}{\widehat{\mu}_{\mathrm{PGA|Collapse}}},$$

$$\widehat{\sigma}_{\ln \mathrm{PGA|Collapse}} = \frac{1}{n-1}\sum_{i=1}^{n}\left(\mathrm{PGA}_i - \widehat{\mu}_{\mathrm{PGA|Collapse}}\right)^2. \tag{15}$$

(2) Nonparametric Analysis Method. A group of ground motion records are selected as the input of the structural seismic collapse analysis (the total number of ground motion records is N_{total}). If there are N_{collapse} ground motion records which lead to the collapse of the structure, then the collapse probability of the structure is $N_{\mathrm{collapse}}/N_{\mathrm{total}}$ under the IM. When the number of ground motion records is sufficient and representative, the collapse probability of the structure can be quantitatively analyzed. The process of collapse seismic fragility analysis of transmission tower based on IDA method is summarized as follows:

(1) The numerical model is established, which can accurately simulate earthquake collapse behavior.

(2) Select a group of ground motion records (the total number is N_{total}), which can reflect the ground motion characteristics of the site, and PGA is selected as IM.

(3) The elastic-plastic time history analysis of the structure is carried out under a certain IM, and the corresponding collapse number of ground motions N_{collapse} can be obtained; finally, the collapse probability of the structure under the IM is expressed as $N_{\mathrm{collapse}}/N_{\mathrm{total}}$.

(4) Monotonically increasing IM and repeating step (3), the collapse probability of the structure under different IMs can be calculated; finally, the structural collapse seismic fragility curve can be obtained.

(5) According to the structural collapse seismic fragility curve, the anticollapse safety and the corresponding reliability of the structure can be evaluated under different earthquake fortification levels.

(3) Collapse Seismic Fragility Analysis. In this paper, according to different earthquake sites and seismic intensity, 12 earthquake ground motion records are selected from the United States PEER strong earthquake record database (Table 7). Figure 20 shows the seismic acceleration response spectrum of record waves with the damping ratio is 2%. It can be seen that the response spectrum of the selected record waves is consistent with that of Chinese code [30]. Thus, 12 earthquake ground motion records are well representative.

The earthquake ground motion is input horizontally along the direction of the transmission tower. By adjusting the PGA amplitude of 12 seismic waves in Table 1, the PGA is adjusted from 0.1 g to 2.5 g and the acceleration increment is 0.1 g, and the PGA of each seismic wave is gradually increased until the transmission tower collapses (the top displacement of tower reaches to $h/80$); substituting the calculated values $\widehat{\mu}_{\ln \mathrm{PGA|Collapse}}$ and $\widehat{\sigma}_{\ln \mathrm{PGA|Collapse}}$ into (14), the collapse fragility curve of the transmission tower can be obtained.

It can be seen from Figure 21 that the seismic collapse probability of the transmission tower increases with the increase of PGA. And the parametric method agrees well with the nonparametric method. According to the Chinese seismic code [30] and seismic fortification standards for transmission towers, the PGA values are 0.11 g, 0.3 g, and 0.51 g under the action of minor earthquakes (exceeding probability is 50%), moderate earthquake (exceeding probability is 10%), and major earthquake (exceeding probability is 2%), respectively. When the collapse probability of the structure is 50%, the corresponding PGA value is 1.43 g using the nonparametric method, while the PGA value is 1.49 g by the parametric method. This value is about 3 times PGA value of major earthquake (the PGA value is 0.3 g). The result indicates that the transmission steel tower has better seismic safety performance and anticollapse ability.

5. Conclusions

This study presents the A general finite particle method framework for collapse simulation of the transmission tower subjected to earthquake ground motions. The FPM is used to establish motion equations of bar elements. Static and dynamic analyses of the transmission tower are conducted using software package MATLAB and ANSYS. Furthermore, failure criteria and the failure modes of structural elements

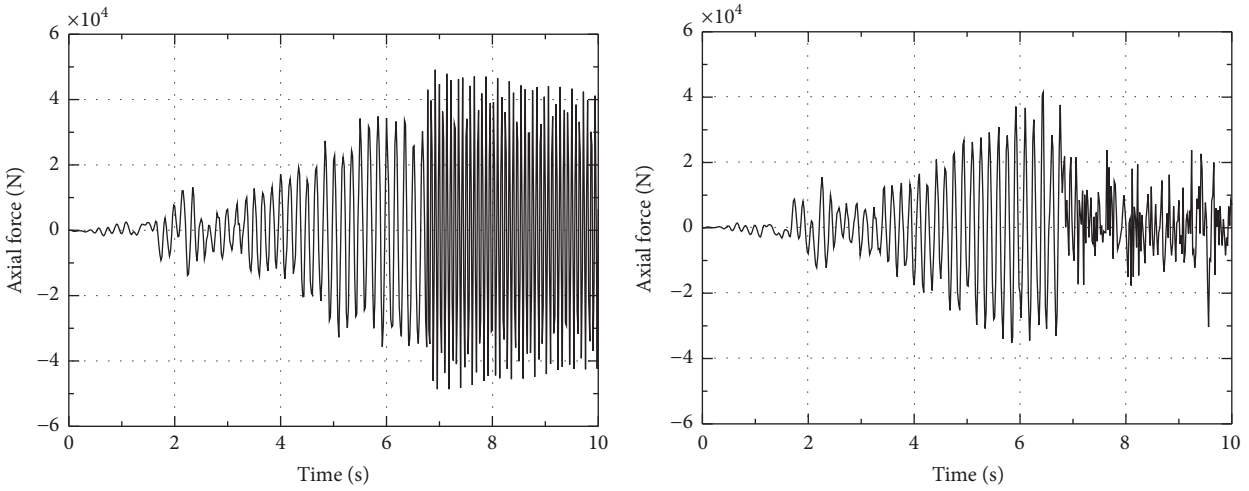

Figure 19: Axial force time history curves of bar elements 139 and 137.

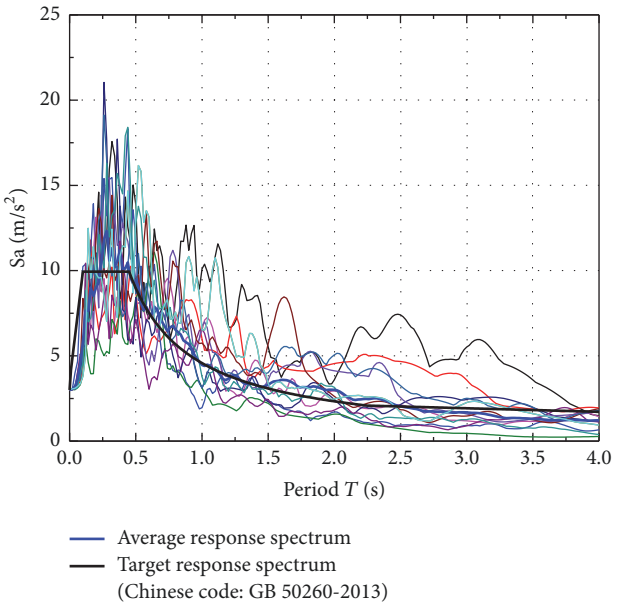

Figure 20: Seismic response spectrum.

are defined. Finally, the process of the transmission tower collapse is simulated. Based on the analysis the following conclusions can be drawn:

(i) The FPM does not need to generate the global stiffness matrix when calculating fracture of members and does not require iterative solution and special amendments in the calculation process; only the number of equations of motion for particles increases. Therefore, the FPM is suitable for solving strong nonlinear dynamic problems such as the seismic collapse analysis of transmission steel tower.

(ii) The model of the transmission tower is established using FEM and FPM, respectively. The correctness of the transmission tower model and the reliability of linear seismic response analysis are verified by comparing the analytical results of the FPM with those of the FEM.

(iii) The material nonlinearity, geometric nonlinearityn and fracture of the truss structure can be well considered in FPM. The collapse processes of the transmission tower are discussed under different PGAs, and the corresponding collapse modes are obtained. The collapse modes will provide a reference to the anticollapse design of the transmission tower subjected to earthquake ground motions.

(iv) The collapse seismic fragility analysis indicates that the parametric method agrees well with the nonparametric method, and seismic collapse probability of

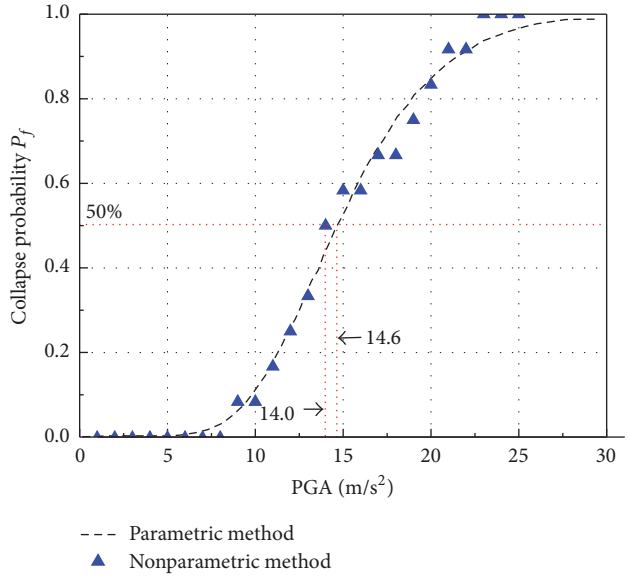

Figure 21: Collapse seismic fragility curves.

the transmission steel tower can meet the demand of Chinese seismic code.

The FPM is advantageous in the simulation of structural failure because particles are free to separate from one another. The collapse processes of the single transmission tower are simulated under one-directional ground motion. Further research on transmission tower-line coupling system and multisupport earthquake excitations can be taken into account in the future. And the reliability of collapse analysis should be verified through experiments or practical failure engineering.

Conflicts of Interest

The authors declare that there are no conflicts of interest regarding the publication of this paper.

Acknowledgments

The authors would like to acknowledge the joint financial support by National Natural Science Fund of China (51278213, 51378234) and the Innovation Foundation of the Fundamental Research Funds for the Central Universities (HUST: 2016YXMS093).

References

[1] F. J. Hall, T. W. Holmes, and P. Somers, "Northridge earthquake, January 17, 1994," Preliminary reconnaissance report, 1994, Preliminary reconnaissance report.

[2] Shinozuka, M. "The Hanshin-Awaji earthquake of January 17, 1995 performance of lifelines," Technical Report NCEER. US National Center for Earthquake Engineering Research (NCEER), 1995, 95.

[3] C. Scawthorn, "The Marmara, Turkey earthquake of August 17, 1999," Reconnaissance Report. Technical Report MCEER, US Multidisciplinary Center for Earthquake Engineering Research, 2000.

[4] Z. Zhang, B. Zhao, and W. Cao, "Investigation and preliminary analysis of damages on the power grid in the Wenchuan earthquake of M8.0," *Electric Power Technologic Economics*, vol. 20, no. 4, pp. 1–4, 2008.

[5] Y. Yu, G. Li, P. Li et al., "Investigation and analysis of electric equipment damage in Sichuan power grid caused by Wenchuan earthquake," *Power System Technology*, vol. 32, no. 11, pp. 1–6, 2008.

[6] D. Zhang, W. Zhao, and M. Liu, "Analysis on seismic disaster damage cases and their causes of electric power equipment in 5·12 Wenchuan earthquake," *Journal of Nanjing University of Technology (National Science Edition)*, vol. 31, no. 1, pp. 44–48, 2009.

[7] L. Kempner, S. Smith, and R. C. Stroud, "Transmission line dynamic/static structural testing," *Journal of the Structural Division*, vol. 107, no. 10, pp. 1895–1906, 1981.

[8] S. L. Chan and S. Kitipornchai, "Geometric nonlinear analysis of asymmetric thin-walled beam-columns," *Engineering Structures*, vol. 9, no. 4, pp. 243–254, 1987.

[9] S. Kitipornchai, K. Zhu, Y. Xiang, and F. G. A. Al-Bermani, "Single-equation yield surfaces for monosymmetric and asymmetric sections," *Engineering Structures*, vol. 13, no. 4, pp. 366–370, 1991.

[10] J. L. Meek and W. J. Lin, "Geometric and material nonlinear analysis of thin-walled beam-columns," *Journal of Structural Engineering (United States)*, vol. 116, no. 6, pp. 1473–1490, 1990.

[11] L. J. Meek and S. Loganathan, "Geometric and material nonlinear behavior of beam-columns," *Computers Structures*, vol. 34, no. 1, pp. 87–100, 1990.

[12] H. Yasui, H. Marukawa, Y. Momomura, and T. Ohkuma, "Analytical study on wind-induced vibration of power transmission towers," *Journal of Wind Engineering & Industrial Aerodynamics*, vol. 83, pp. 431–441, 1999.

[13] Q. Lin, W. Wang, D. Cao et al., "Progressive collapse analysis of high-voltage transmission tower under earthquake action," *Sichuan Building Science*, vol. 40, no. 3, pp. 157–161, 2014.

[14] Z. J. Zhang, G. H. Paulino, and W. Celes, "Extrinsic cohesive modelling of dynamic fracture and microbranching instability in brittle materials," *International Journal for Numerical Methods in Engineering*, vol. 72, no. 8, pp. 893–923, 2007.

[15] X. Lu, X. Lin, and L. Ye, "Simulation of structural collapse with coupled finite element-discrete element method," in *Computational Structural Engineering*, pp. 127–135, Springer, Netherlands, 2009.

[16] Y. Luo and C. Yang, "The finite particle method for solving geometric large deformation of planar solids," *Engineering Mechanics*, vol. 30, no. 4, pp. 260–268, 2013.

[17] W.-L. Jin and T. Fang, "Numerical simulation of failure behavior of reinforced concrete frame structures by discrete element method," *Gongcheng Lixue/Engineering Mechanics*, vol. 22, no. 4, pp. 67–73, 2005.

[18] F. Zhang and X. Lv, "Numerical simulation and analysis of different collapse patterns for RC frame structure," *Journal of Building Structures*, vol. 30, no. 5, pp. 119–125, 2009.

[19] E. C. Ting, C. Shih, and Y.-K. Wang, "Fundamentals of a vector form intrinsic finite element: Part I. Basic procedure and a plane frame element," *Journal of Mechanics*, vol. 20, no. 2, pp. 113–122, 2004.

[20] E. C. Ting, C. Shih, and Y.-K. Wang, "Fundamentals of a vector form intrinsic finite element: Part II. Plane solid elements," *Journal of Mechanics*, vol. 20, no. 2, pp. 123–132, 2004.

[21] W. J. Lewis, M. S. Jones, and K. R. Rushton, "Dynamic relaxation analysis of the non-linear static response of pretensioned cable roofs," *Computers & Structures*, vol. 18, no. 6, pp. 989–997, 1984.

[22] Y. Yu, G. H. Paulino, and Y. Luo, "Finite particle method for progressive failure simulation of truss structures," *Journal of Structural Engineering*, vol. 137, no. 10, pp. 1168–1181, 2011.

[23] C. D. Hill, G. E. Blandford, and S. T. Wang, "Post-buckling analysis of steel space trusses," *Journal of Structural Engineering (United States)*, vol. 115, no. 4, pp. 900–919, 1989.

[24] K. M. Lynn and D. Isobe, "Structural collapse analysis of framed structures under impact loads using ASI-Gauss finite element method," *International Journal of Impact Engineering*, vol. 34, no. 9, pp. 1500–1516, 2007.

[25] H.-D. Zheng, J. Fan, and X.-H. Long, "Analysis of the seismic collapse of a high-rise power transmission tower structure," *Journal of Constructional Steel Research*, vol. 134, pp. 180–193, 2017.

[26] M. Papadrakakis, "Post-buckling analysis of spatial structures by vector iteration methods," *Computers & Structures*, vol. 14, no. 5-6, pp. 393–402, 1981.

[27] W. J. Baker and C. A. Cornell, "Vector-valued ground motion intensity measures for probabilistic seismic demand analysis," PEER Report 10, 2006.

[28] M. Sasani and A. Der Kiureghian, "Seismic fragility of RC structural walls: displacement approach," *Journal of Structural Engineering*, vol. 127, no. 2, pp. 219–228, 2001.

[29] DL/T 5154-2012, *Technical code for design of tower and pole structures of overhead transmission line*, China Planning Press, Beijing, China, 2012.

[30] GB 50260-2013, *Code for Seismic Design of Power Installations*, China Planning Press, China, 2013.